Insight into Prolonged Cycling Life of 4 V All-Solid-State Polymer Batteries by a High-Voltage Stable Binder

Jianneng Liang, Dachang Chen, Keegan Adair, Qian Sun, Nathaniel Graham Holmes, Yang Zhao, Yipeng Sun, Jing Luo, Ruying Li, Li Zhang, Shangqian Zhao, Shigang Lu, Huan Huang, Xiaoxing Zhang, Chandra Veer Singh, and Xueliang Sun**

Polyethylene oxide (PEO) based solid polymer electrolytes (SPEs) are incompatible with the 4 V class cathodes such as $LiCoO_2$ due to the limited electrochemical oxidation window of PEO. Herein, a number of binders including commonly used binders PEO, polyvinylidene fluoride (PVDF), and carboxyl-rich polymer (CRP) binders such as sodium alginate (Na-alginate) and sodium carboxymethyl cellulose, are studied for application in the 4 V class all-solid-state polymer batteries (ASSPBs). The results show ASSPBs with CRP binders exhibit superior cycling performance up to 1000 cycles (60% capacity retention, almost 10 times higher than those with PEO and PVDF binders). Synchrotron-based X-ray absorption spectroscopy (XAS), morphology studies and density functional theory studies indicate that, with their carboxyl groups, CRPs can strongly bind the electrode materials together, and work as coating materials to protect the cathode/SPE interface. Cyclic voltammetry studies indicate that CRP binders are more stable at high voltage compared to PEO and PVDF. The stability under high voltage and the coating property of CRP binders contribute to stable cathode/SPE interfaces as disclosed by the X-ray photoelectron spectroscopy and Co L-edge XAS results, enabling long cycling life, high performance 4 V class ASSPBs.

1. Introduction

Lithium-ion batteries (LIBs) play an integral role in our daily life, with a wide variety of applications extending from portable electronic devices to electric vehicles. However, the organic liquid electrolyte used in conventional LIBs presents serious safety concerns due to its flammability and low flash-point.[1] The development of solid-state batteries (SSBs) is a promising direction for addressing these safety issues. One of the key components of high-performance SSBs is the solid-state electrolyte (SSE). Oxide-based SSEs,[2] sulfide-based SSEs,[3] halide-based SSEs,[4] polymer-based SSEs,[5] and hybrid electrolytes[6] are regarded as the most encouraging candidates for applications in SSBs.[7] Among them, polyethylene oxide (PEO) based solid polymer electrolytes (SPEs) show great promising due to its high ionic conductivity at elevated temperature, low interfacial resistance toward electrodes, and simple fabrication process.[8] More importantly, all-solid-state polymer batteries (ASSPBs) with lithium metal anode, SPE and $LiFePO_4$ cathode have been commercialized and used in the Bolloré Bluecar,[5] which clearly demonstrates the great capability of SPE for SSBs for EV application.

However, it has been found that the state-of-the-art PEO-based SPEs developed so far delivered poor electrochemical performance when coupling with high energy density cathodes, such as lithium cobalt oxide ($LiCoO_2$), layer structure lithium nickel manganese cobalt oxide (NMC), and lithium nickel cobalt aluminum oxide (NCA).[9] This is because PEO-based SPEs have a relatively low electrochemical oxidation potential—less than 3.8 V versus Li/Li+.[10] However, these high energy density cathodes typically require charging voltages up to 4.2 V or higher to achieve a high specific capacity. At these voltages range, PEO-based SPEs will undergo electrochemical oxidation decomposition.[10,11] In order to address this serious limitation, significant research efforts

Dr. J. Liang, K. Adair, Q. Sun, N. G. Holmes, Dr. Y. Zhao, Y. Sun, J. Luo, R. Li, Prof. X. Sun
Department of Mechanical and Materials Engineering
University of Western Ontario
London, ON N6A 5B9, Canada
E-mail: xsun9@uwo.ca
D. Chen, Prof. C. V. Singh
Department of Materials Science and Engineering
University of Toronto
Toronto, ON M5S 3E4, Canada
E-mail: chandraveer.singh@utoronto.ca

The ORCID identification number(s) for the author(s) of this article can be found under https://doi.org/10.1002/aenm.202002455.

D. Chen, Prof. X. Zhang
Department School of Electrical Engineering and Automation
Wuhan University
Wuhan 430072, China
Dr. L. Zhang, Dr. S. Zhao, Dr. S. Lu
China Automotive Battery Research Institute Co, Ltd
Beijing 101407, China
Dr. H. Huang
Glabat Solid-State Battery Inc
700 Collip Circle, Suite 211, London, ON N6G 4×8, Canada
Prof. X. Zhang
Department School of Electrical and Electronic Engineering
Hubei University of Technology
Wuhan 430068, China

have been dedicated to stabilizing the SPEs when coupling with 4 V class cathodes. They can be classified to the following strategies: i) The first approach is coating the cathode particles with inert materials which are stable at high voltage, such as Al_2O_3,[12] Li_3PO_4,[13] polymer materials (including PECA[14] and CMC[15]), and NASICON SSE (LATP)[11,16] and LAGP.[17] ii) The second method is coating the whole cathode electrode using techniques such as atomic layer deposition to deposit materials such as lithium tantalite,[18] lithium niobate.[19] iii) The third strategy involves making double layer SPEs with a SPE stable at high voltage on the cathode side and a SPE stable at low voltage adjacent to the Li metal anode,[20] or using the same polymer metric with different lithium salt at different layer.[21] Although many of the above-mentioned methods can enhance the cycling stability and increase the cycling life of ASSPBs using 4 V class cathodes, they usually require additional complicated treatment steps, and they still cannot achieve long-term cycling performance.

The binder in the electrode plays many critical roles including: i) both a dispersing agent and a thickener for a homogeneous distribution of electrode components; ii) bridge between particles and a current collector via certain mechanical, intermolecular, or chemical forces to maintain mechanical integrity; iii) maintainer of electronic contact upon cycling; and iv) modifier of the wettability and facilitator of ionic transport at the electrode/electrolyte interface.[22] In SSBs, the ionic conductivity of electrode and the binding between solid-state active material particles are poor. The binder in the SSBs' electrode should not only bridge the active material particles and/or carbon particles together to maintain intimate contact,[23] but also facilitate the ionic transport at the interface.[23f,24] Also, some ASSPBs operate at an elevated temperature. Therefore, the binder should be stable at a wide working temperature range and maintain the mechanical integrity. Chemical and electrochemical stabilities of binder during operation process are also very important. The binder should not be oxidized or reduced during charge/discharge process, and it should not be dissolved into electrolyte, or the SSE should be indissoluble in the polymer binder.

Unfortunately, in ASSPBs, the ionic conductivity of the binder is overemphasized, since the ionic conductivity of the cathode is poor without infiltration of liquid electrolyte. Thus, the most commonly used binders in ASSPBs are PEO or ethylene oxide (EO)-containing polymers which have good ionic conductivity at elevated temperature.[2b,5,12,14,25] However, PEO and EO-containing polymers have a low electrochemical oxidation potential, and low melting point, which makes them unsuitable for 4 V class ASSPBs. It is therefore necessary to pursue a suitable binder for long cycle life, high performance high voltage ASSPBs.

Herein, we will introduce a facile and highly effective method by simply adopting the high voltage tolerant binders to significantly prolong the cycling lives of 4 V class ASSPBs based on PEO-based SPEs. We conducted a careful study which examined the suitability of different binders including PEO, polyvinylidene fluoride (PVDF), and two kind of carboxyl-rich polymer (CRP) binders (including sodium alginate (Na-alginate) and sodium carboxymethyl cellulose (CMC)) for 4 V class $LiCoO_2$ electrodes which were then coupled with PEO-based SPEs for

assembling ASSPBs. The electrochemical performance results show that ASSPBs with CRP binders (CMC) can maintain 85% capacity after 300 cycles and 59.7% after 1000 cycles, which are significantly higher than those of ASSPBs with PEO or PVDF binder. The insight mechanism was investigated by combining with different advanced characterization techniques. Synchrotron-based X-ray absorption spectroscopy (XAS) on O K-edge and the morphologies studies shows that CRPs can strongly bind the electrode materials together and work as a coating material. Density functional theory result also confirms the strong binding between CRPs and $LiCoO_2$ original from the strong absorption between carboxyl group and $LiCoO_2$, which is well agreement with XAS and morphologies results. Cyclic voltammetry (CV) studies indicate that CRP binders are more stable at high voltage polymer batteries compared to PEO and PVDF. Electrochemical impedance spectroscopy (EIS), X-ray photoelectron spectroscopy (XPS), and Co L-edge XAS results demonstrate that a stable SPE/cathode interface is achieved with the CRP binder, while obvious PEO decomposition products are observed in the SPE/$LiCoO_2$ electrode interface with PEO as the binder. The high voltage stability and coating property of CRP binders in 4 V class cathodes throughout the charge and discharge process are the important steps on the road to high-performance, long cycle life, 4 V class ASSPBs.

2. Result and Discussions

$LiCoO_2$ (LCO) electrodes with different binders were all prepared by a slurry casting method with an active material, binder, and acetylene black (AB) ratio of 8:1:1 by weight. Figures S1–S4 (Supporting Information) show the scanning electron microscope (SEM) and corresponding energy dispersive X-ray spectroscopy (EDX) mapping for LCO electrodes with PEO (referred to as PEO–LCO), PVDF (referred to as PVDF–LCO), Na-alginate (referred to as Na-alginate-LCO), and CMC (referred to as CMC–LCO) binders. Figures S5–S6 present the Raman and XRD spectra of LCO electrodes. The cycling performances of these ASSPBs with different binders made LCO electrodes were evaluated by galvanostatic charge–discharge cycling at 60 °C. The results are presented in **Figure 1**. The initial discharge capacity delivered by PEO–LCO is 135.3 mAh g^{-1} at 0. 1 C, slightly higher than the 134.4, 130.9, and 131.8 mAh g^{-1} delivered by PVDF–LCO, Na-alginate–LCO and CMC–LCO, respectively. The discharge capacities delivered by these ASSPBs are comparable to that obtained from liquid-based LCO batteries (Figure S7, Supporting Information). Figure 1a,b shows the charge/discharge profiles for these ASSPBs with PEO and CRP (CMC) as the binders at different charge/discharge cycles (from 3 to 100). For PEO–LCO, a significant decrease in the charge/discharge capacity and an obvious increase in the overpotential are observed. However, for CMC–LCO, no decrease in the charge/discharge capacity or increase in the overpotential are observed, indicating that the ASSPB fabricated with CMC binder are more stable than that fabricated with PEO binder. As shown in Figure 1d,e, after 300 cycles, 40.1% capacity is retained for the PEO–LCO ASSPB, 46% for the PVDF–LCO ASSPB, and 85% for the CMC–LCO ASSPB. After 1000 cycles, the capacity retention of PEO–LCO ASSPB is only 6.7%, while
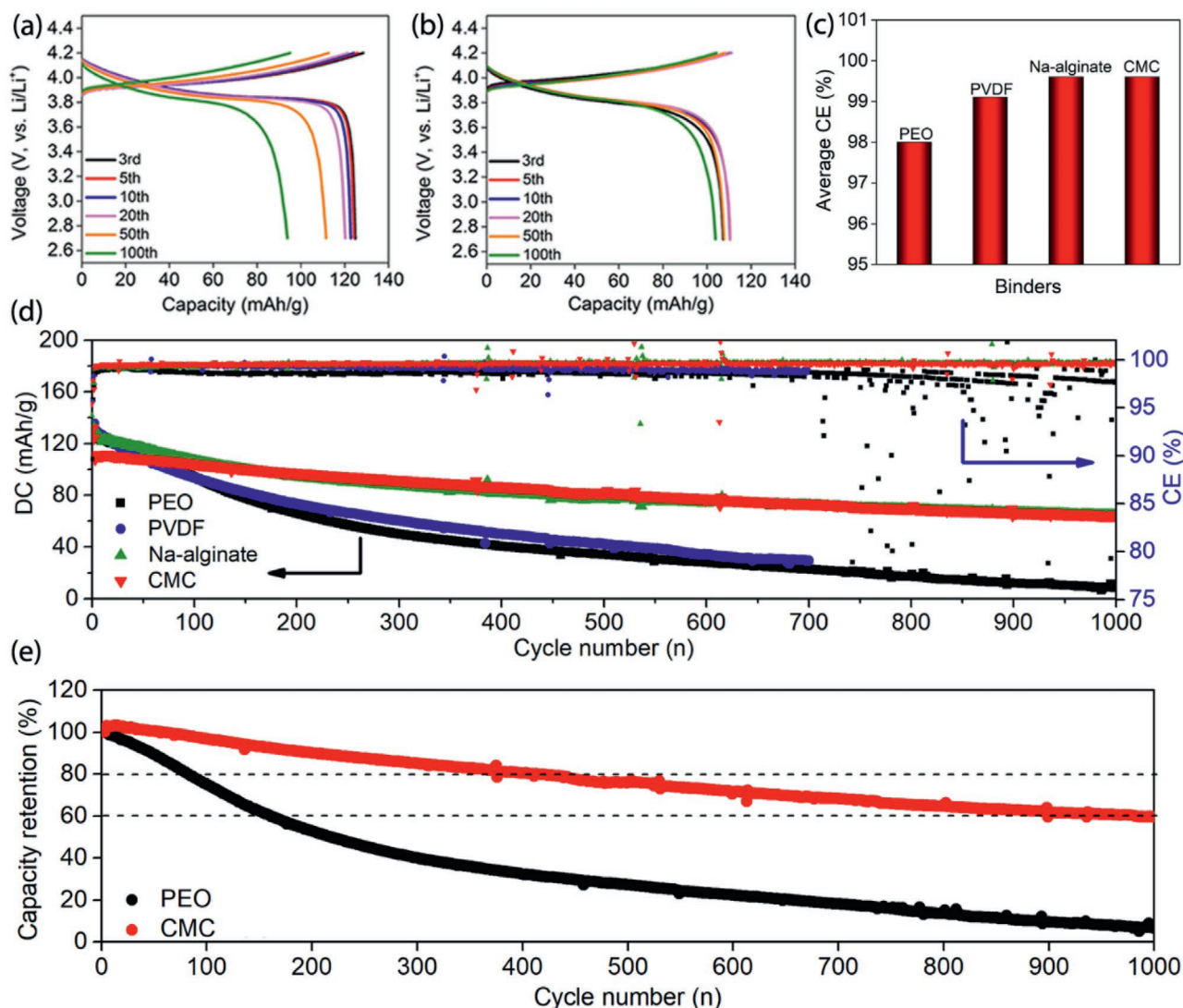
Figure 1. Electrochemical performance evaluations of ASSPBs. The charge/discharge voltage profiles of a) PEO–LCO, b) CMC–LCO ASSPBs from 3 to 100 cycles. c) The average Coulombic efficiency of ASSPBs with different binders after 1000 cycles. d) Cycle performance of ASSPBs with different binders. e) Capacity retention of ASSPBs with PEO and CMC as the binders after 1000 cycles. Capacity retention is calculated as a percentage of the discharge capacities over the third cycle discharge capacity. (DC: Discharge Capacity, CE: Coulombic Efficiency) All batteries were tested at 60 °C with a voltage cut off of 2.7–4.2 V, and a current density of 0.1 C for the first three cycles and 0.4 C for the remaining cycles.

59.7% capacity remains for the CMC–LCO ASSPB. Similar performance were achieved for Na-alginate–LCO ASSPB, clearly demonstrating that CRPs binders have superior performance in high voltage ASSPBs.

The initial and average Coulombic efficiencies of these ASSPBs after 1000 cycles are compared in Figure S8 (Supporting Information); and Figure 1c, respectively. After 1000 charge/discharge cycles, the average Coulombic efficiency for PEO–LCO, PVDF–LCO (700 cycles), Na-alginate–LCO, and CMC–LCO is 98.0%, 99.1%, 99.6%, and 99.6%, respectively. The lower average Coulombic efficiencies of PEO–LCO and PVDF–LCO indicate the more serious electrochemical decomposition of the binders or PEO-based SPE in these ASSPBs systems.

The charge voltage cut-off up to 4.3 V was also investigated and similarly, better cycling performances of ASSPBs with

Na-alginate and CMC CRP binders are observed and poorer performances were achieved in PEO and PVDF binders ASSPBs (Figure S9, Supporting Information).

To investigate the underlying mechanism responsible for the performance enhancement associated with different binders, CV, EIS, SEM, synchrotron-based soft XAS, the density functional theory (DFT) calculation, and XPS were performed to study the physical/electrochemical properties of CRP binders, PEO and PVDF binders as well as the interfacial properties between LCO and SPEs.

The electrochemical stabilities of PEO, PVDF, Na-alginate, and CMC polymers were evaluated and compared using CV method.[26] The results are shown in Figure S11 (Supporting Information). The cells contain lithium metal as the counter electrode, PEO-based SPE as the lithium ion conductor and separator, and 70 wt% binder + 30 wt% acetylene black (AB)
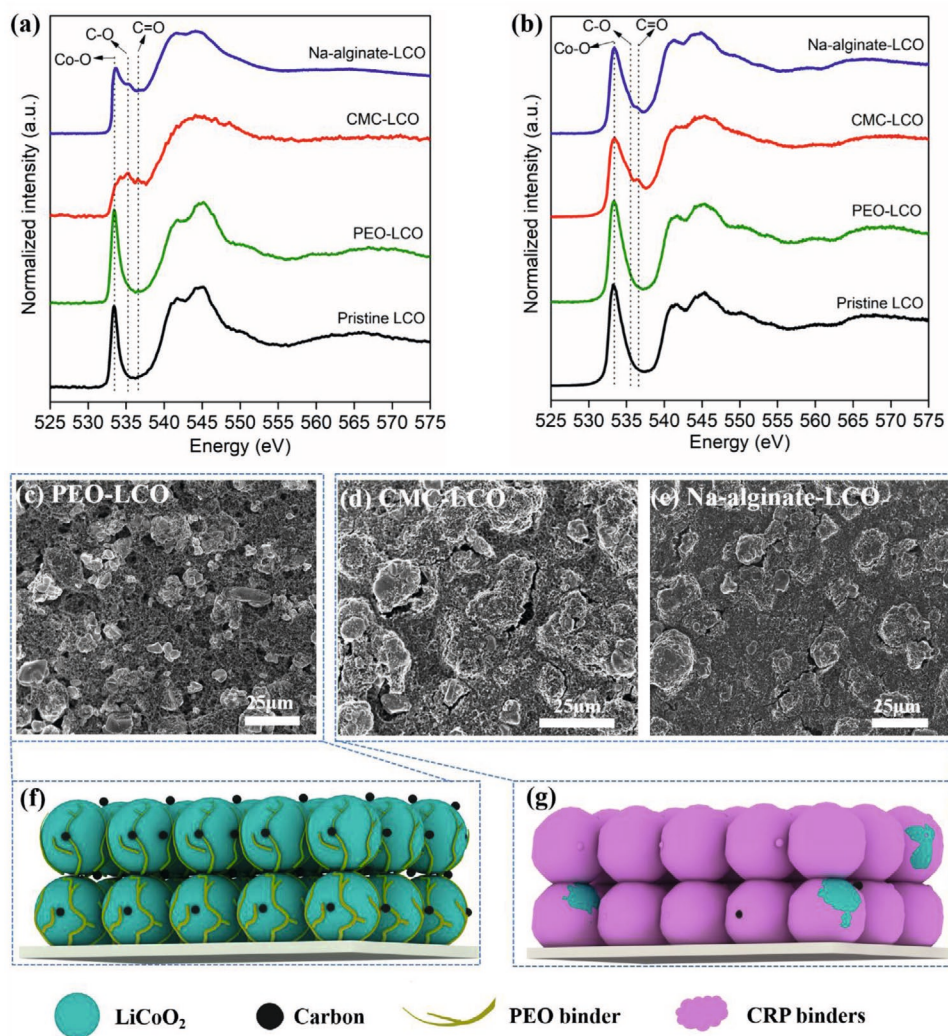
ADVANCED
SCIENCE NEWS
www.advancedsciencenews.com

ADVANCED
ENERGY
MATERIALS
www.advenergymat.de

Figure 2. O K-edge XAS at a) TEY mode and b) FLY mode for different LiCoO$_2$ samples. SEM images for c) PEO–LCO, d) CMC–LCO, and e) Na-alginate-LCO electrodes. f) Schematic diagrams for the binding capability/mechanism of PEO f) and CRP binders g).

composite electrode as the working electrode. CV was conducted at 60 °C with 0.2 mV s^{-1} scan rate, scanning from open circuit voltage to 4.3 V and then back to 3 V. An outstanding CV anodic current intensity from PEO cell, compared to the PVDF, Na-alginate, and CMC cells, suggests a more significant electrochemical decomposition of PEO binder may occur if the cell was charged to 4.3 V. PVDF binder also shows a very high anodic current intensity compared to these CRP binders. The electrochemical decomposition process is not reversible since not a corresponding cathodic peak at CV cure is observed. Which means the decomposition products may accumulate, resulting in thicker cathodic electrolyte interphase (CEI) layer in cathode/SPE interface upon cycling, which is detrimental to the performances of ASSPBs. The trend of CV anodic current intensity for different binders is consistent well with the long cycling performances of ASSPBs shown in Figure 1, which means the decomposition of binder may be the key reason for the performance fading in 4 V class ASSPBs. A high voltage stable binder can help to achieve a high-performance and long cycling life 4 V class ASSPB.

XAS at the O K-edge was performed for studying the chemical/physical properties of LCO electrodes with different binders and the results are shown in **Figure 2**. Spectra were collected with two detection modes, total electron yield (TEY) and fluorescence yield (FLY). TEY mode collected information about a depth of a few nanometers (2–10 nm) from the sample surface while FLY is more bulk sensitive, collecting information deeper (over 100 nm) into the sample.[27] For TEY information (Figure 2a), the spectrum of PEO–LCO electrode is almost the same as that of pristine LCO particles, which means that, on the PEO–LCO electrode surface, there is not PEO covering on LCO particle surface to influence the Co–O peak intensity. This phenomenon discloses the following information: during the PEO–LCO electrode drying process, because of the poor binding of PEO on LCO surface, PEO flows down to the bottom of electrode. Therefore, on the surface of electrode, no/few PEO exits, and LCO particles are "naked", as a result, no XAS peak corresponding to PEO arise and the Co–O XAS peak is as strong as it is in pristine LCO particles sample. However, for CRP binders based LCO electrodes, the peaks related to
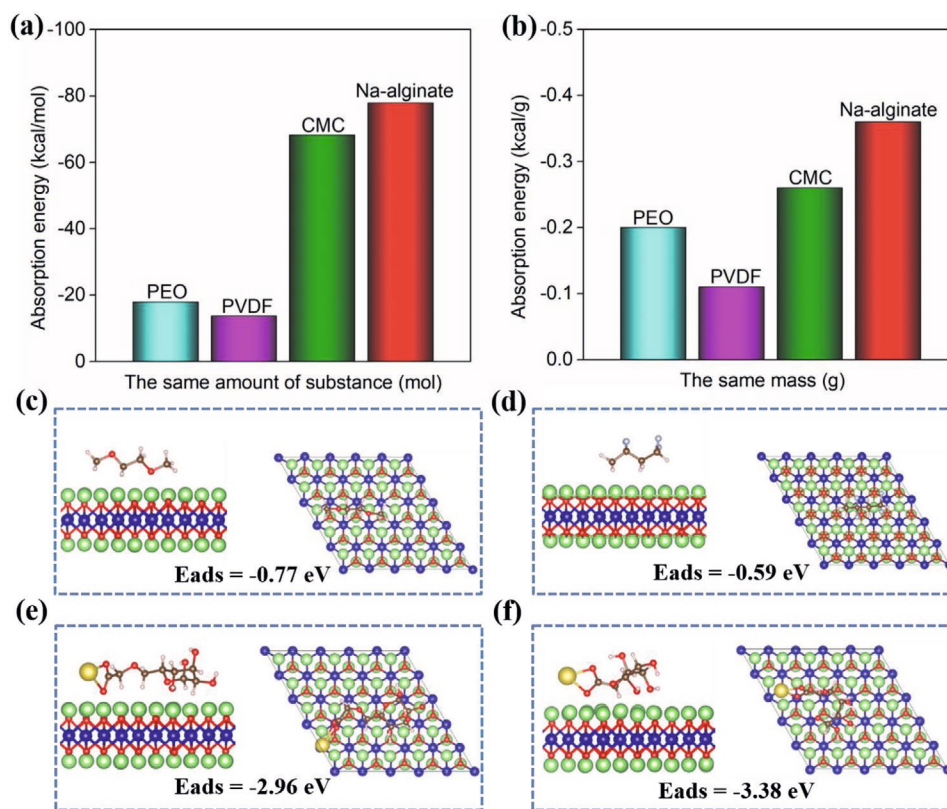
Figure 3. a) Adsorption energy comparison with the same molar quantity and b) mass quantity g). Optimized geometric structure and adsorption energy comparison c) PEO dipolymer, d) PVDF (dipolymer), e) CMC monomer, and f) Sodium alginate monomer on LiCoO$_2$ (001).

C−O and C=O structure (from Na-alginate or CMC) are out-standing,[28] while the Co−O peak intensity from LCO decrease compared to that of pristine LCO particles. This indicates that there are CRP binders covering the surfaces of LCO particles on the CRP binders-LCO electrode surface. In other word, CRPs work as coating-like materials on LCO particle surface. For FLY information (Figure 2b), similar conclusions can be obtained as compared to TEY spectra (Figure 2a).

The morphologies of these electrodes are characterized by SEM to further support the conclusion from O K-edge XAS results. PEO–LCO electrode surface (Figure 2c) shows very loose and porous structure. The surface of LCO particles on the top of electrode are clear without carbon black particles adhesive, which means the poor binding ability of PEO. However, for CMC–LCO and Na-alginate–LCO electrodes, their morphologies are less porous and big amount of carbon black particles landing on LCO particles surface, meaning CRP binders can strongly bridge the carbon particles and LCO particles together (Figure 2d,e).

Combining the SEM results and the O K-edge XAS results, the binding effects of PEO and CRPs binders are then schematically illustrated in Figure 2f,g. PEO binder has poor binding capability, as a result of this, PEO binder will drop down to the bottom of electrode during the electrode drying process. Therefore, on the surface of PEO–LCO electrode, there is not/ few PEO, thus LCO particle surface is exposed. In contrast, the CRPs binders have strong capacity to adhesive on LCO particle surface and binding capacity. Therefore, they can not

only strongly bridge the carbon and LCO particles together for maintaining the integrity of electrodes, but also work as coating material to protect electrode/SPE interface and to avoid the decomposition of PEO-based SPE at high voltage, therefore, rendering a ultrastable high performance 4 V class ASSPB.

To determine the atomic mechanism behind the improved performance of CPRs binders over PEO and PVDF binders, the interface properties between binders and LCO were further investigated by DFT. The details of the DFT study are listed in the Supporting Information. The adsorption energy and the structure of the binders adsorbed on the surface of LCO (001) are shown in **Figure 3**. For the CMC monomer and Na-alginate, the adsorption energies of –68.26 and –77.85 kcal mol^{-1}, respectively, are computed to be much larger than the same amount of PEO and PVDF dipolymers (Figure 3a). The charge transfer between four polymers and the surface are: 0.58e for PEO dipolymer, 0.21e for PVDF dipolymer, 1.25e for CMC monomer, and 2.03e for Na-alginate monomer, and all of the monomer/dipolymer accept electrons. Because the polymer will not directly participate in the charge/discharge process, the charge transfer has little effect on the performance of the battery, and the stability mainly depends on the binding/adsorption energy between polymers and the surface. Although the CMC and Na-alginate show much larger adsorption energies, their molar masses vary greatly. We therefore normalized the adsorption energy for all adsorptions. The normalized adsorption energy (kcal g^{-1}) comparison is shown in Figure 3b, demonstrating that the CMC and Na-alginate have stronger chemical interactions with the LCO

ADVANCED
SCIENCE NEWS
www.advancedsciencenews.com

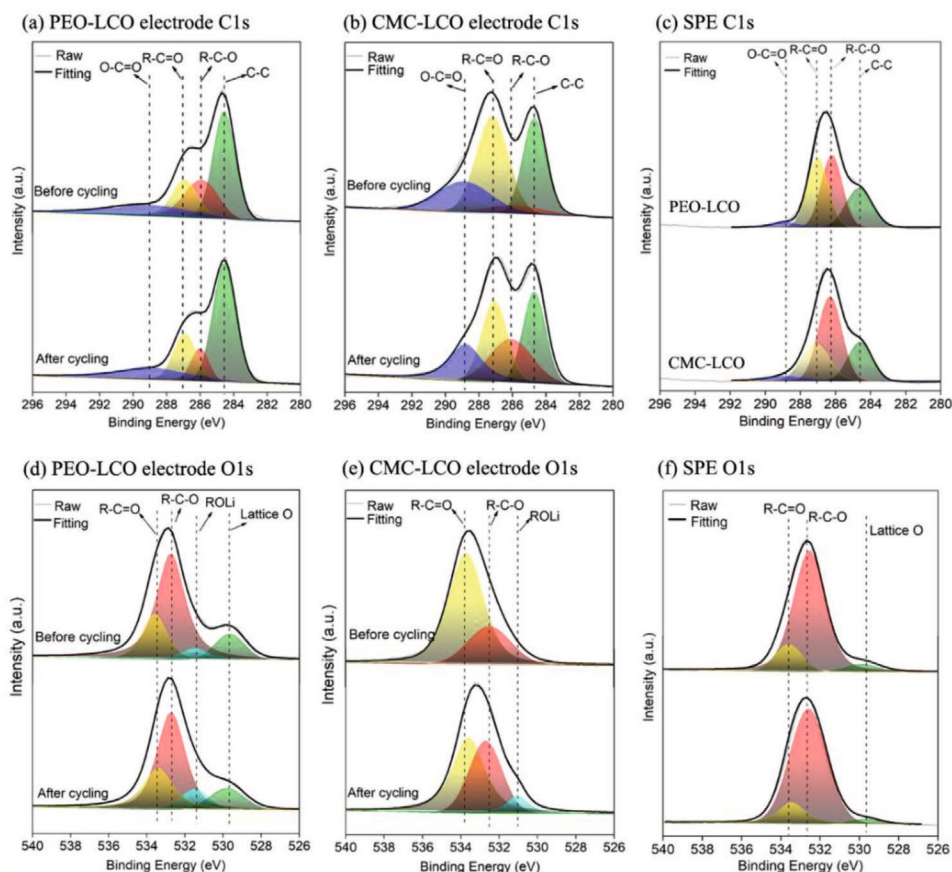ADVANCED
ENERGY
MATERIALS
www.advenergymat.de

Figure 4. XPS study of SPE/LiCoO$_2$ electrode interface. C 1s from a) PEO–LCO electrode surface and b) CMC–LCO electrode surface. c) C 1s from SPE surface after cycling with PEO–LCO electrode and CMC–LCO electrode. O 1s from d) PEO–LCO electrode surface and e) CMC–LCO electrode surface; f) O 1s from SPE surface after cycling with PEO–LCO electrode and CMC–LCO electrode. Cycled samples were obtained from the ASSPBs after cycling for 5 cycling (at discharge state).

(001) surface compared to PEO and PVDF. The charge density difference (CDD) configurations of PEO and CMC adsorption are shown in Figure S13 (Supporting Information). Electron accumulation is found to occur between the carboxyl Na atom in CMC and the LCO surface. Meanwhile, the O atoms in PEO and CMC show electron accumulation around them, but to a lower degree than around carboxyl Na atom. The total density of states of the entire structures and the partial density of states of the adsorbed PEO and CMC are shown in Figure S14 (Supporting Information). The states from −17.5 to −7.5 eV are mainly from the adsorbed species, with a small contribution from the surface, indicating orbital overlapping in this energy range. The DFT simulation results suggest that stronger chemical interactions exist between the LCO surface and CRPs binders, demonstrating better binding capacity of CRPs binders in 4 V class ASSPBs compared to PEO and PVDF. These results are well consistent with the O K-edge XAS and SEM results in Figure 2 and cycling performance results in Figure 1.

The interfacial properties between LCO electrodes and PEO-based SPE were investigated by XPS, EIS, and XAS. The C 1s and O 1s XPS results at LCO electrodes surfaces and cycled SPEs surface (face to cathode side) are shown in **Figure 4**. As shown in Figure 4a, before and after cycling, PEO–LCO

have similar XPS C 1s spectra, which were fitted to C−C ($\approx$284.5 eV), R−C−O ($\approx$285.9 eV), R−C=O ($\approx$287.2 eV), O−C=O ($\approx$288.9 eV).[29] The C−C peak at 284.5 eV can be assigned to the conductive carbon. The R−C−O peak can be assigned to PEO binder, since the PEO molecular structure consists of HO−[CH$_2$−CH$_2$−O]$_n$−H molecular fragments. R−C=O and O−C=O peaks could be the result from the reaction/interaction between PEO and LCO. This is supported by the Co L-edge XAS results in Figure 6; and Figure S15 (Supporting Information). Compared to pristine LCO particles, the low energy shoulder peak intensity at 776–778 eV of PEO–LCO electrode sample is much higher, which means Co is reduced by PEO, PEO is oxidized by LCO. More detailed discussion will be presented in the content below. The O−C=O peak could be also resulted from Li$_2$CO$_3$ impurity on LiCoO$_2$ particles, since there will be Li$_2$CO$_3$/LiOH formation once LiCoO$_2$ was exposed to air.[30] This is also supported by the O 1s result in Figure 4d where there is ROLi (LiOH) peak in the no-cycled PEO-LCO electrode.

The R−C−O peak intensity/area in C 1s XPS spectrum decreases, whereas, R−C=O peak intensity/area increases, and the intensity/area of O−C=O peak also increase after cycling for the PEO–LCO electrode (Figure 4a). The increase of

ADVANCED
SCIENCE NEWS
www.advancedsciencenews.com

ADVANCED
ENERGY
MATERIALS
www.advenergymat.de

R—C=O and O—C=O peak intensity/area could be the result of the decomposition products of PEO, which contains R—C=O or O—C=O segment.[31] The increase of intensities/areas at R—C=O and O—C=O peaks after cycling for PEO–LCO electrode are also supported by the O 1s results (Figure 4d) where the R—C=O peak intensity/area increases obviously after cycling. ROLi is detected by O 1s in both uncycled and cycled PEO–LCO electrodes. The formation of ROLi may arise from the interaction between PEO and LiCoO$_2$ and the LiOH impurity. ROLi peak increased in intensity/area after cycling, which means the decomposition of PEO may result in Li-containing products such as LiOH or other RO–Li-type polymeric-organic species.[29c] All these results indicate serious decomposition of PEO at the interface between the PEO–LCO electrode and SPE, resulting in an unstable CEI layer.

XPS C 1s and O 1s results of CMC–LCO electrodes before and after cycling are shown in Figure 4b,e. Similar peaks assignments were used for fitting the spectra as before. For C 1s of CMC–LCO electrode before cycling, the R—C—O, R—C=O, O—C=O peaks arise from the LiOH/Li$_2$CO$_3$ impurity and CMC polymer binder. Moreover, the R—C—O peak increases greatly after cycling, due to the residue of PEO-based SPE on the electrode surface (after the electrode is peeled off from the SPB). The R—C—O peak in O 1s spectrum is also increased, which is consistent with the C 1s result. No increase in R—C=O, O—C=O peaks is observed in both C 1s and O 1s results after cycling, which suggests better stability of the SPE and/or the binder at high potentials. A minor ROLi peak arises from the CMC–LCO electrode after cycling is possibly due to the interaction between PEO-based SPE and LCO.

The C 1s, O 1s XPS spectra of SPE surface (toward cathode electrode) in Figure 4c,f show that the R—C=O peak intensity/area is higher in PEO–LCO ASSPB than that in CMC–LCO ASSPB. It also support the conclusion that there is more decomposition of SPE/PEO binder at the cathode/SPE interface in PEO–LCO electrode.

The significant lattice O peak in Figure 4d indicates the exposure of LCO particles on the surface of PEO–LCO electrode, while the absence of lattice O peak in Figure 4e implies full coverage of LCO particles by the CMC binder in CMC-LCO electrode. This further confirms the coating effect of CMC on LCO particles, as consistent with the results presented in Figure 2.

Overall, not/less decomposed products of PEO-based SPE at the CMC–LCO electrode surface was detected, which is probably because that CRPs binders are higher voltage stable and work as coating materials to protect the cathode/SPE interface and eliminate the detrimental effect of carbon in accelerating the electrochemical decomposition of PEO-based SPE.

The decomposition of binder or SPE at the SPE/electrode interface will result in the formation of CEI layer and increase of the cell impedance. EIS was then conducted to evaluate the impedance of the ASSPBs with different binders and the results are presented in **Figure 5**. Though the cell with PEO binder has smaller cell impedance within 20 cycles, its impedance increases grammatically with the increase of the cycle number. It is over 2000 Ω after 200 cycles of charge/discharge. The continuous increase of the cell impedance indicates that the SPE/electrode interface is not stable and continue decomposition of SPE or binder occur at the interface. In contrast, the impedance of the cell with CMC binder is very stable. Even after 200 cycles, its value still maintains at around 770 Ω as it is at first cycle, which indicates that the SPE/electrode interface is very stable at the cell with CMC binder.

XAS at the Co L-edge was conducted to study the variation in surface chemical properties of LCO before and after charging. The results are presented in **Figure 6**. The Co L$_{3,2-edge}$ XAS spectrum consists of two main peaks corresponding to the transitions of Co 2p$_{3/2}$ and 2p$_{1/2}$ to unoccupied 3d states, respectively.[32] The TEY measurements of both the PEO–LCO and CMC–LCO electrodes exhibit similar Co L-edge features compared to that of pristine LCO particles. The Co L-edge XAS spectrum of pristine LCO particles confirms the oxidation state of Co is 3+, as expected.[33] However, an obvious difference is observed at the low energy shoulder (778.5 eV) of the L$_3$ peak. The increase of the shoulder peak intensity means a decrease in the unoccupied high-energy Co 3d state, indicating that Co is reduced.[34] In Figure 5a, both the PEO–LCO and CMC–LCO electrodes have a higher L$_3$ lower energy shoulder peak intensity compared to that of a pristine LCO particle. This is possibly due to the interaction/reaction between the PEO and CMC polymer with the LCO surface, resulting in the reduction of surficial Co, similar to the reaction between liquid organic electrolytes and LCO.[35] However, after cycling, the L$_3$ lower energy shoulder intensity increases more significantly for
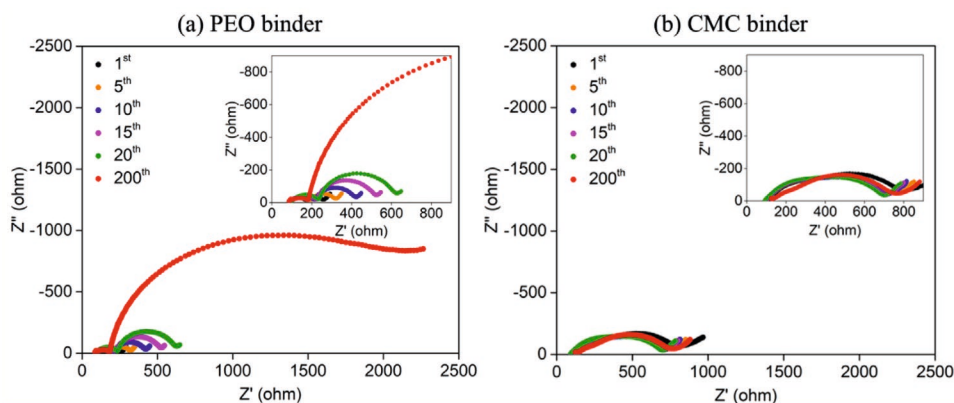

Figure 5. EIS study of ASSPBs with different binders. Nyquist plots of a) ASSPB with PEO as the binder and b) CMC as the binder after different charge/discharge cycles.
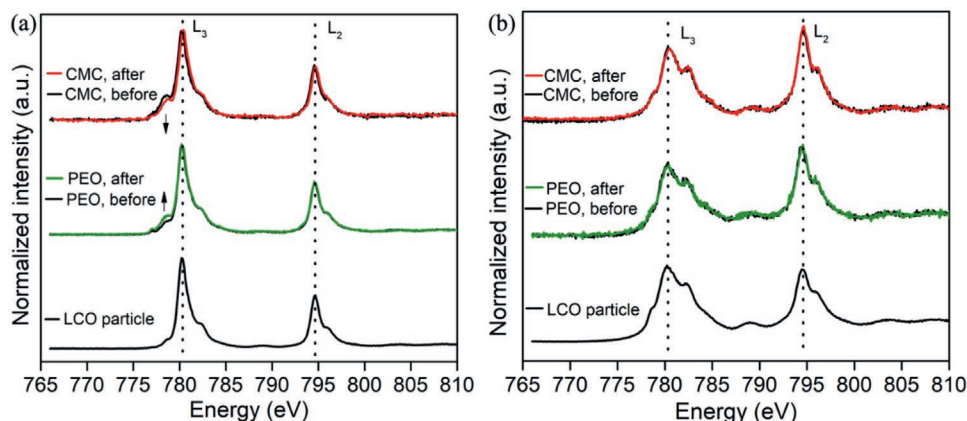
ADVANCED
SCIENCE NEWS
www.advancedsciencenews.com

ADVANCED
ENERGY
MATERIALS
www.advenergymat.de

Figure 6. Synchrotron-based XAS at Co L-edge at discharge state with a) TEY detection and b) FLY detection for LCO particles, PEO–LCO electrodes, and CMC–LCO electrodes before and after 5 cycles at full discharge state.

PEO–LCO, indicating that surficial reduction of LCO by PEO is propagating during the charge/discharge process, leading to an unstable PEO/LCO interface. In contrast, after cycling, the L_3 lower energy shoulder of the CMC–LCO electrode decreases in intensity, indicating that the surface interaction/reaction between the LCO and CMC binder may be reversible. This result illustrates that CMC/LCO has better interfacial stability compared to the PEO/LCO interface. Thus CMC can work as a good coating material to protect LCO/PEO-based SPE interface. From the FLY measurements (Figure 6b), no obvious difference was found in the Co XAS spectra, which suggests the reactions are isolated to the near-surface regions and the bulk of the $LiCoO_2$ is unaffected by these parasitic side reactions.

3. Conclusion

Overall, we show that the alternation of binders can dramatically improve the cycling stability of PEO-based ASSPBs. To demonstrate, four different binders including PEO, PVDF, and carboxyl-rich polymer binders (including Na-alginate and CMC) have been studied for the applications in 4 V class ASSPBs with LCO cathodes, lithium metal anodes and PEO-based SPEs. Results show that carboxyl-rich polymers are better binders for high-performance and long cycle life. Mechanism studies indicate that PEO binder has poor binding capacity and is easily electrochemical decomposed at high voltage, while carboxyl-rich polymers binders are more stable in the same operating voltage window. The strong chemical absorption between carboxyl-rich polymer binders and the LCO make these binders can not only strongly bind the carbon and LCO particles together for maintaining the structure stability of electrodes, but also work as a coating material to protect electrode/SPE interface and avoid the electrochemical decomposition of PEO-based SPE. Therefore, carboxyl-rich polymers binders can dramatically improve the performance and cycling life of high voltage ASSPBs. This study provides new insight for developing high-performance, long cycle life, 4 V class solid polymer batteries, paving the way for high energy density SSBs for electric vehicle applications.

4. Experimental Section

Preparation of PEO-Based SPE: PEO (M.W. 1 000 000), $LiClO_4$ (purity, 99.9%) and garnet-type SSE ($Li_{6.4}La_3Zr_{1.4}Ta_{0.6}O_{12}$, LLZTO, home-made) were carefully dried at 50 °C before use. 0.12 g of LLZTO was mixed with 25 mL of acetonitrile (AN) and ultrasonicated for 6 h. 0.6 g of PEO and 0.19 g of $LiClO_4$ were then added into the mixture and stirred for 12 h. The homogeneous mixture was then cast onto a Teflon substrate and the solvent was slowly evaporated at room temperature first, and SPE was then transferred to a 60 °C vacuum oven for 2 days. The obtained PEO–$LiClO_4$–LLZTO SPE membrane was then immediately transferred to an Ar-protected glovebox and left to rest for 3 days or longer before use.

$LiCoO_2$ Electrodes and Binder-AB Composite Electrodes Preparation: $LiCoO_2$ electrodes were prepared by mixing 80 wt% $LiCoO_2$ particles, 10 wt% carbon-black (Acetylene Black (AB)), 10 wt% binder (PEO, PVDF, Na-alginate, CMC,) and solvent to form a slurry. A doctor blade casting method was used to coat the slurry on the carbon coated Al foil. The PEO–LCO, Na-alginate–LCO, and CMO–LCO electrodes were dried at 60 °C in a vacuum oven for 12 h and the PVDF–LCO electrode was dried at 100 °C in a vacuum oven for 12 h to obtain the LCO electrodes. Binder-AB composite electrodes were prepared by mixing 70 wt% polymer binder (PEO, PVDF, Na-alginate, or CMC, respectively) with 30 wt% AB powders in solvent to form a slurry that was subsequently coated onto the carbon-coated Al foil by a doctor blade casting method and dried in a vacuum oven overnight. The loading of binder in the binder-AB composite electrodes was around 0.3 mg cm^{-2}. The solvent was AN for the PEO, N-methylpyrrolidinone (NMP) for PVDF, and water for Na-alginate and CMC.

Electrochemical Performance Testing: ASSPBs were assembled in 2032 type coin cells in an Ar-protected glove box (Vacuum Atmosphere Company, moisture and oxygen level less than 1 ppm). $LiCoO_2$ electrodes with different binders and lithium foils were used as the working electrodes and the counter electrodes. The PEO–$LiClO_4$–LLZO SPEs were used as both ionic conductor and separator. No additional solvent or liquid electrolyte was used in the $LiCoO_2$ ASSPBs. The size of the cathode and lithium anode electrodes were 10 mm in diameter. The size of SPE was 12.7 mm in diameter. Galvanostatic charge/discharge testing was performed between 2.7 and 4.2 V (or 4.3 V) in a 60 °C oven using a LAND Battery Tester. All ASSPBs were rested for over 30 h before testing. Cyclic Voltammetry of the ASSPBs was performed between 2.7 and 4.2 V (vs Li/Li$^+$) in a 60 °C oven. For liquid based $LiCoO_2$ batteries, a liquid electrolyte containing 1 M $LiPF_6$ in ethylene carbonate (EC), ethylmethyl carbonate (EMC), and diethyl carbonate (DEC) solvents with a 1:1:1 volume radio was used and Celgard 2400 was used as the separator. All the liquid based $LiCoO_2$ batteries were tested at room

temperature with a current density of 0.1 C for first two cycles and 0.5 C at the rest of cycles.

Material Characterizations: A Hitachi S-4800 field emission scanning electronic microscope (FE-SEM) equipped with EDX was used to characterize the morphology and elemental distribution in samples. XPS was conducted with a Thermo Scientific K-Alpha instrument at the University of Toronto. XAS measurements using TEY and FLY modes at the Co K-edge were collected at the Canadian light source (CLS). Pristine $LiCoO_2$ powders and uncycled $LiCoO_2$ electrodes (with binder and AB) were used directly as the samples for XPS and XAS analyses. Cycled $LiCoO_2$ electrodes and cycled SPE samples were obtained from the cycled ASSPBs (53 °C, 0.02 C current density, 5 cycles) by separating the SPE layer and $LiCoO_2$ electrode. Raman spectra were collected in Renishaw inVia Raman microscope, laser wavelength = 514.5 nm. XRD were collected in Bruker D8 Advance Diffractometer XRD system.

Theoretical Method: Density functional theory studies details are illustrated in the Supporting Information.

Supporting Information

Supporting Information is available from the Wiley Online Library or from the author.

Conflict of Interest

The authors declare no conflict of interest.

Author Contributions

J.L. and D.C. contributed equally to this work. J.L., Q.S., and X.S. conceived the idea and experiments; J.L. and Q.S. conducted the synthesis of electrodes and SPEs, electrochemical performance testing, SEM, XPS, and synchrotron samples preparations. D.C. and C.V.S. designed and conducted theoretical calculations. K.A. helped with the synchrotron testing. J.L., N.G.H., Y.Z., Y.S., R.L., X.L.Z., S.L., H.H., and X.Z. participated in the data analysis and discussion. X.S. and C.V.S., respectively, supervised the experimental and simulations parts of the project. All authors discussed the results and commented on the manuscript.

[1] K. Liu, Y. Liu, D. Lin, A. Pei, Y. Cui, *Sci. Adv.* **2018**, *4*, eaas9820.

[2] a) V. Thangadurai, S. Narayanan, D. Pinzaru, *Chem. Soc. Rev.* **2014**, *43*, 4714; b) R. Murugan, V. Thangadurai, W. Weppner, *Angew. Chem., Int. Ed.* **2007**, *46*, 7778.

[3] a) N. Kamaya, K. Homma, Y. Yamakawa, M. Hirayama, R. Kanno, M. Yonemura, T. Kamiyama, Y. Kato, S. Hama, K. Kawamoto, A. Mitsui, *Nat. Mater.* **2011**, *10*, 682; b) Y. Kato, S. Hori, T. Saito, K. Suzuki, M. Hirayama, A. Mitsui, M. Yonemura, H. Iba, R. Kanno, *Nat. Energy* **2016**, *1*, 16030.

[4] a) T. Asano, A. Sakai, S. Ouchi, M. Sakaida, A. Miyazaki, S. Hasegawa, *Adv. Mater.* **2018**, *30*, 1803075; b) X. Li, J. Liang, N. Chen, J. Luo, K. R. Adair, C. Wang, M. N. Banis, T.-K. Sham, L. Zhang, S. Zhao, S. Lu, H. Huang, R. Li, X. Sun, *Angew. Chem., Int. Ed.* **2019**, *58*, 16427; c) X. Li, J. Liang, J. Luo, M. Norouzi Banis, C. Wang, W. Li, S. Deng, C. Yu, F. Zhao, Y. Hu, T.-K. Sham, L. Zhang, S. Zhao, S. Lu, H. Huang, R. Li, K. R. Adair, X. Sun, *Energy Environ. Sci.* **2019**, *12*, 2665.

[5] P. Hovington, M. Lagacé, A. Guerfi, P. Bouchard, A. Mauger, C. M. Julien, M. Armand, K. Zaghib, *Nano Lett.* **2015**, *15*, 2671.

[6] a) T. Jiang, P. He, G. Wang, Y. Shen, C.-W. Nan, L.-Z. Fan, *Adv. Energy Mater.* **2020**, *10*, 1903376; b) J. Liang, J. Luo, Q. Sun, X. Yang, R. Li, X. Sun, *Energy Storage Mater.* **2019**, *21*, 308.

[7] a) W. Zhao, J. Yi, P. He, H. Zhou, *Electrochem. Energy Rev.* **2019**, *2*, 574; b) X. Yang, X. Li, K. Adair, H. Zhang, X. Sun, *Electrochem. Energy Rev.* **2018**, *1*, 239.

[8] Z. Xue, D. He, X. Xie, *J. Mater. Chem. A* **2015**, *3*, 19218.

[9] H. Zhang, J. Zhang, J. Ma, G. Xu, T. Dong, G. Cui, *Electrochem. Energy Rev.* **2019**, *2*, 128.

[10] Y. Xia, T. Fujieda, K. Tatsumi, P. P. Prosini, T. Sakai, *J. Power Sources* **2001**, *92*, 234.

[11] K. Nie, X. Wang, J. Qiu, Y. Wang, Q. Yang, J. Xu, X. Yu, H. Li, X. Huang, L. Chen, *ACS Energy Lett.* **2020**, *5*, 826.

[12] H. Miyashiro, Y. Kobayashi, S. Seki, Y. Mita, A. Usami, M. Nakayama, M. Wakihara, *Chem. Mater.* **2005**, *17*, 5603.

[13] S. Seki, Y. Kobayashi, H. Miyashiro, Y. Mita, T. Iwahori, *Chem. Mater.* **2005**, *17*, 2041.

[14] J. Ma, Z. Liu, B. Chen, L. Wang, L. Yue, H. Liu, J. Zhang, Z. Liu, G. Cui, *J. Electrochem. Soc.* **2017**, *164*, A3454.

[15] T. Kobayashi, Y. Kobayashi, M. Tabuchi, K. Shono, Y. Ohno, Y. Mita, H. Miyashiro, *ACS Appl. Mater. Interfaces* **2013**, *5*, 12387.

[16] a) Q. Yang, J. Huang, Y. Li, Y. Wang, J. Qiu, J. Zhang, H. Yu, X. Yu, H. Li, L. Chen, *J. Power Sources* **2018**, *388*, 65; b) J. Qiu, X. Liu, R. Chen, Q. Li, Y. Wang, P. Chen, L. Gan, S.-J. Lee, D. Nordlund, Y. Liu, X. Yu, X. Bai, H. Li, L. Chen, *Adv. Funct. Mater.* **2020**, *30*, 1909392.

[17] Z. Li, A. Li, H. Zhang, R. Lin, T. Jin, Q. Cheng, X. Xiao, W.-K. Lee, M. Ge, H. Zhang, A. Zangiabadi, I. Waluyo, A. Hunt, H. Zhai, J. J. Borovilas, P. Wang, X.-Q. Yang, X. Chuan, Y. Yang, *Nano Energy* **2020**, *72*, 104655.

[18] J. Liang, Y. Sun, Y. Zhao, Q. Sun, J. Luo, F. Zhao, X. Lin, X. Li, R. Li, L. Zhang, S. Lu, H. Huang, X. Sun, *J. Mater. Chem. A* **2020**, *8*, 2769.

[19] J. Liang, S. Hwang, S. Li, J. Luo, Y. Sun, Y. Zhao, Q. Sun, W. Li, M. Li, M. Norouzi Banis, X. Li, R. Li, L. Zhang, S. Zhao, S. Lu, H. Huang, D. Su, X. Sun, *Nano Energy* **2020**, *78*, 105107.

[20] W. Zhou, Z. Wang, Y. Pu, Y. Li, S. Xin, X. Li, J. Chen, J. B. Goodenough, *Adv. Mater.* **2019**, *31*, 1805574.

[21] C. Wang, T. Wang, L. Wang, Z. Hu, Z. Cui, J. Li, S. Dong, X. Zhou, G. Cui, *Adv. Sci.* **2019**, *6*, 1901036.

[22] a) H. Chen, M. Ling, L. Hencz, H. Y. Ling, G. Li, Z. Lin, G. Liu, S. Zhang, *Chem. Rev.* **2018**, *118*, 8936; b) H. Yuan, J.-Q. Huang, H.-J. Peng, M.-M. Titirici, R. Xiang, R. Chen, Q. Liu, Q. Zhang, *Adv. Energy Mater.* **2018**, *8*, 1802107.

[23] a) K. Lee, J. Lee, S. Choi, K. Char, J. W. Choi, *ACS Energy Lett.* **2019**, *4*, 94; b) K. Lee, S. Kim, J. Park, S. H. Park, A. Coskun, D. S. Jung, W. Cho, J. W. Choi, *J. Electrochem. Soc.* **2017**, *164*, A2075; c) J. Zhang, H. Zhong, C. Zheng, Y. Xia, C. Liang, H. Huang, Y. Gan, X. Tao,

W. Zhang, *J. Power Sources* **2018**, *391*, 73; d) N. C. Rosero-Navarro, T. Kinoshita, A. Miura, M. Higuchi, K. Tadanaga, *Ionics* **2017**, *23*, 1619; e) K. H. Park, Q. Bai, D. H. Kim, D. Y. Oh, Y. Zhu, Y. Mo, Y. S. Jung, *Adv. Energy Mater.* **2018**, *8*, 1800035; f) Z. Wan, D. Lei, W. Yang, C. Liu, K. Shi, X. Hao, L. Shen, W. Lv, B. Li, Q.-H. Yang, F. Kang, Y.-B. He, *Adv. Funct. Mater.* **2019**, *29*, 1805301.

[24] R.-J. Chen, Y.-B. Zhang, T. Liu, B.-Q. Xu, Y.-H. Lin, C.-W. Nan, Y. Shen, *ACS Appl. Mater. Interfaces* **2017**, *9*, 9654.

[25] X. Yang, Q. Sun, C. Zhao, X. Gao, K. R. Adair, Y. Liu, J. Luo, X. Lin, J. Liang, H. Huang, L. Zhang, R. Yang, S. Lu, R. Li, X. Sun, *Nano Energy* **2019**, *61*, 567.

[26] F. Han, Y. Zhu, X. He, Y. Mo, C. Wang, *Adv. Energy Mater.* **2016**, *6*, 1501590.

[27] J. Xu, E. Hu, D. Nordlund, A. Mehta, S. N. Ehrlich, X.-Q. Yang, W. Tong, *ACS Appl. Mater. Interfaces* **2016**, *8*, 31677.

[28] a) J. Ren, F. Weber, F. Weigert, Y. Wang, S. Choudhury, J. Xiao, I. Lauermann, U. Resch-Genger, A. Bande, T. Petit, *Nanoscale* **2019**, *11*, 2056; b) N. Bonnet-Mercier, R. A. Wong, M. L. Thomas, A. Dutta, K. Yamanaka, C. Yogi, T. Ohta, H. R. Byon, *Sci. Rep.* **2014**, *4*, 7127.

[29] a) A. N. Mansour, D. G. Kwabi, R. A. Quinlan, Y.-C. Lu, Y. Shao-Horn, *J. Electrochem. Soc.* **2016**, *163*, A2911; b) R. Tatara, P. Karayaylali, Y. Yu, Y. Zhang, L. Giordano, F. Maglia, R. Jung, J. P. Schmidt, I. Lund, Y. Shao-Horn, *J. Electrochem. Soc.* **2019**, *166*,

A5090; c) D. J. Xiong, R. Petibon, L. Madec, D. S. Hall, J. R. Dahn, *J. Electrochem. Soc.* **2016**, *163*, A1678.

[30] Y. Ji, P. Zhang, M. Lin, W. Zhao, Z. Zhang, Y. Zhao, Y. Yang, *J. Power Sources* **2017**, *359*, 391.

[31] a) L. Yang, F. Heatley, T. G. Blease, R. I. G. Thompson, *Eur. Polym. J.* **1996**, *32*, 535; b) P. de Sainte Claire, *Macromolecules* **2009**, *42*, 3469.

[32] W.-S. Yoon, K.-B. Kim, M.-G. Kim, M.-K. Lee, H.-J. Shin, J.-M. Lee, J.-S. Lee, C.-H. Yo, *J. Phys. Chem. B* **2002**, *106*, 2526.

[33] Y. Ma, Y. Zhou, C. Du, P. Zuo, X. Cheng, L. Han, D. Nordlund, Y. Gao, G. Yin, H. L. Xin, M. M. Doeff, F. Lin, G. Chen, *Chem. Mater.* **2017**, *29*, 2141.

[34] a) F. Lin, I. M. Markus, D. Nordlund, T.-C. Weng, M. D. Asta, H. L. Xin, M. M. Doeff, *Nat. Commun.* **2014**, *5*, 3529; b) F. Lin, D. Nordlund, T. Pan, I. M. Markus, T.-C. Weng, H. L. Xin, M. M. Doeff, *J. Mater. Chem. A* **2014**, *2*, 19833; c) F. Lin, D. Nordlund, Y. Li, M. K. Quan, L. Cheng, T.-C. Weng, Y. Liu, H. L. Xin, M. M. Doeff, *Nat. Energy* **2016**, *1*, 15004.

[35] a) D. Takamatsu, Y. Koyama, Y. Orikasa, S. Mori, T. Nakatsutsumi, T. Hirano, H. Tanida, H. Arai, Y. Uchimoto, Z. Ogumi, *Angew. Chem., Int. Ed.* **2012**, *51*, 11597; b) Y. Orikasa, D. Takamatsu, K. Yamamoto, Y. Koyama, S. Mori, T. Masese, T. Mori, T. Minato, H. Tanida, T. Uruga, Z. Ogumi, Y. Uchimoto, *Adv. Mater. Interfaces* **2014**, *1*, 1400195.